Elsevier Editorial System(tm) for Inorganica Chimica Acta
Manuscript Draft

Manuscript Number: ICA-D-12-00158R1

Title: Cisplatin drug delivery using gold-coated iron oxide nanoparticles for enhanced tumour targeting with external magnetic fields

Article Type: SI: Metals in Medicine

Keywords: cisplatin; iron oxide; gold; nanoparticle; drug delivery; magnetic

Corresponding Author: Dr Nial Wheate,

Corresponding Author's Institution:

First Author: Amelia J Wagstaff

Order of Authors: Amelia J Wagstaff; Sarah D Brown; Megan R Holden; Gemma E Craig; Jane A Plumb; Norbert Schreiter; Roisin E Brown; Wojciech Chrzanowski; Nial J Wheate, PhD

*Graphical Abstract (pictogram)

Click here to download high resolution image

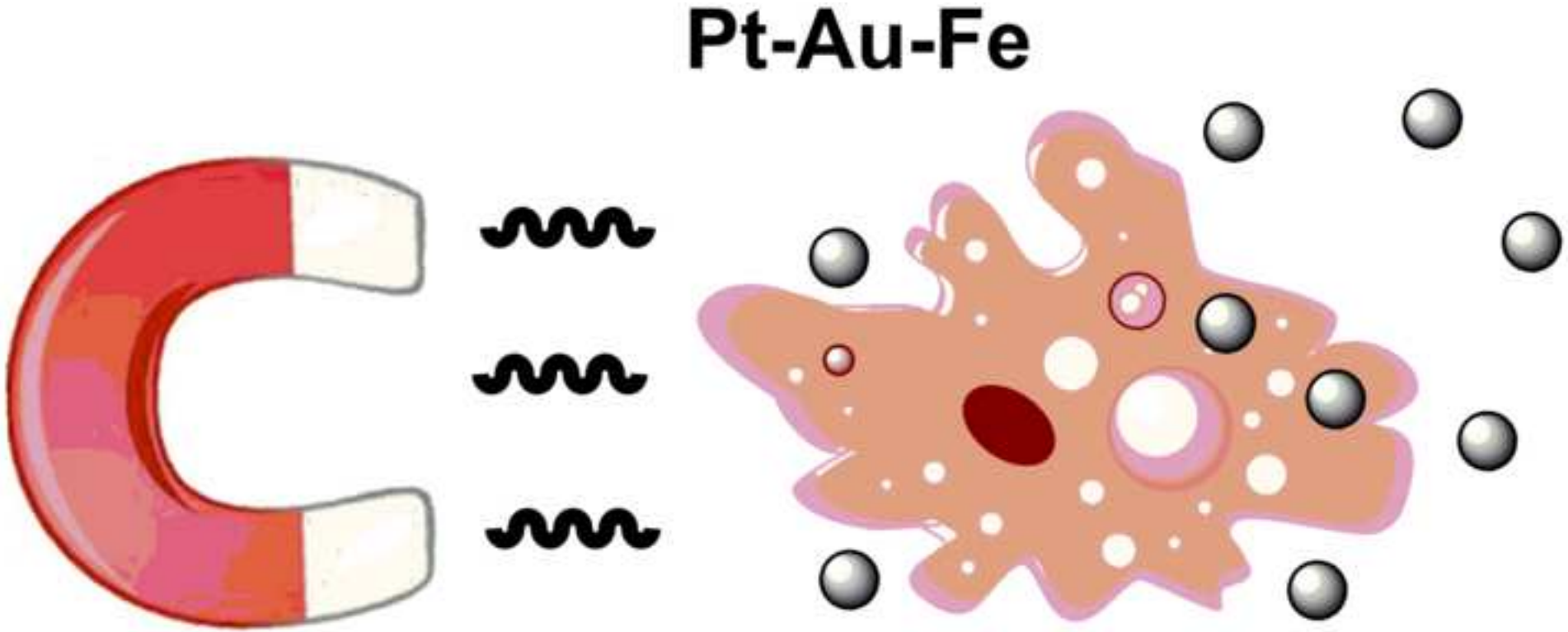

***Graphical abstract (synopsis)**

Gold-coated iron oxide nanoparticles with tethered platinum drug have been developed in an effort to produce a means of directing the movement and localisation of drugs in chemotherapy directly to the sites of solid tumours using external magnetic fields.

***Highlights**

- Gold-coated iron oxide nanoparticles have been synthesised to which the active component of cisplatin has been attached.
- The nanoparticles are highly cytotoxic in the ovarian carcinoma cell lines A2780 and A2780/cp70.
- The nanoparticles can be controlled and moved by an external magnetic field to site specifically inhibit cancer cell growth.
- The results demonstrate a potential ability to direct drugs in the human body in cancer treatment, thus greatly reducing the severity of drug side-effects.

Cisplatin drug delivery using gold-coated iron oxide nanoparticles for enhanced tumour targeting with external magnetic fields

Amelia J. Wagstaff,[1] Sarah D. Brown,[2] Megan R. Holden,[2] Gemma E. Craig,[2] Jane A. Plumb,[3] Roisin E. Brown,[2] Norbert Schreiter,[2] Wojciech Chrzanowski,[1*] Nial J. Wheate[1]*

[1] Faculty of Pharmacy,
The University of Sydney,
NSW, 2006, Australia.

[2] Strathclyde Institute of Pharmacy and Biomedical Sciences,
University of Strathclyde,
161 Cathedral Street,
Glasgow, G4 0RE,
United Kingdom.

[3] Institute of Cancer Studies,
College of Medicine, Veterinary and Life Sciences,
University of Glasgow,
Cancer Research UK Beatson Laboratories,
Garscube Estate, Glasgow, G61 1BD,
United Kingdom.

***** e-mail: nial.wheate@sydney.edu.au; wojciech.chrzanowski@sydney.edu.au; fax: +61 2 9351 4391

Keywords: Iron oxide, gold, nanoparticle, cisplatin, cancer, magnet, cytotoxicity.

Abstract

The platinum-based chemotherapeutic drug cisplatin is highly effective in the treatment of solid tumours, but its use is restricted by poor bioavailability, severe dose-limiting side effects and rapid development of drug resistance. In light of this we have tethered the active component of cisplatin to gold-coated iron oxide nanoparticles to improve its delivery to tumours and increase its efficacy. Iron oxide nanoparticles (FeNPs) were synthesised via a co-precipitation method before gold was reduced onto its surface (Au@FeNPs). Aquated cisplatin was used to attach $\{Pt(NH_3)_2\}$ to the nanoparticles by a thiolated polyethylene glycol linker forming the desired product (Pt@Au@FeNP). The nanoparticles were characterised by dynamic light scattering, scanning transmission electron microscopy, UV visible spectrophotometry, inductively coupled plasma mass spectrometry and electron probe microanalysis. The nanoparticles increase in size as they are constructed, with the synthesised FeNPs having a diameter of 5-50 nm, which increases to 20-80 nm for the Au@FeNPs, and to 60-120 nm for the Pt@Au@FeNPs. Nanoparticle drug loading was found to be 7.9×10^{-4} moles of platinum per gram of gold. The FeNPs appear to have little inherent cytotoxicity, whereas the Au@FeNPs are as active as cisplatin in the A2780 and A2780/cp70 cancer cell lines. More importantly the Pt@Au@FeNPs are up to 110-fold more cytotoxic than cisplatin. Finally, external magnets were used to demonstrate that the nanoparticles could be accumulated in specific regions and that cell growth inhibition was localised to those areas.

1. Introduction

Cisplatin, *cis*-diamminodichloridoplatinum(II), is the most effective platinum based drug for the treatment of solid tumours [1-3]. It is indicated first line in malignancies of the lung, ovary, head and neck, bladder and cures over 90% of testicular cancers [1]. Cisplatin is activated when it enters the cell and subsequently binds directly to DNA, disrupting replication and transcription, which triggers an apoptotic response [1]. Following injection of cisplatin, most of the drug is excreted renally with only a fraction of the remaining dose converted to the active diaquo-platinum form [1], limiting the amount of drug that actually binds to DNA. The use of cisplatin is also restricted due to intrinsic and acquired resistance caused by reduced drug uptake and efflux, increased detoxification via thiol-containing biomolecules, and increased DNA repair [1, 4, 5]. Additionally, it displays significant dose-related side effects such as nephrotoxicity, neurotoxicity, and nausea and vomiting, which can be attributed to its indiscriminate attack on both healthy and cancerous cells [6].

Nanoparticle-based drug delivery vehicles have the ability to overcome some of these limitations by passively or actively targeting tumours. The disorganised vasculature and absence of effective lymphatic drainage in solid tumours allows nanoparticles to leak from the blood stream and accumulate in the cancer, a phenomenon known as the Enhanced Permeability and Retention (EPR) effect [7]. This allows nanoparticles to target tumours passively, reducing uptake into healthy cells.

Recently, tumour targeting using magnetic fields to direct the movement and localisation of drugs to solid tumours has generated much interest [8]. Magnetic nanoparticles offer the benefit of utilising both the EPR effect (passive targeting) whilst also ensuring a direct, guided delivery to the tumour (active targeting). Nanoparticles of iron oxide possess superparamagnetic properties, whereby magnetism is only present when under direct energy from an external magnetic field [9]. Other advantages of iron oxide include its ability to be used in magnetic resonance imaging and induce cytotoxicity through near

infrared induced hyperthermia [10]. Unfortunately, iron oxide alone in physiological media is unstable, resulting in oxidation, aggregation and precipitation [10-13]. Moreover, it is a challenge to attach molecules to the surface of iron oxide. On attachment of cisplatin to iron oxide nanoparticles, it was observed that the drug rapidly dissociated due to inefficient binding [14]. In vivo, this may result in early release of cisplatin whilst still in the blood stream and failure of the drug to reach the tumour [14]. Similar fast release of cisplatin from iron oxide nanoparticles has been observed in a number of other studies as well [15, 16]. There is therefore a need to develop safer, more stable iron oxide nanoparticles that can retain platinum drugs more strongly on their surfaces.

The use of gold nanoparticles as chemotherapeutic drug delivery vehicles is attractive as it is non-toxic, non-immunogenic, and provides a highly tunable surface to which drugs can be attached [17-19]. Previously we demonstrated that the active components of cisplatin and oxaliplatin can be tethered to gold nanoparticles with a drug loading of up to 60,000 cisplatin-like molecules per nanoparticle [20, 21]. In addition, the oxaliplatin-nanoparticle conjugate showed a 6-fold increase in cytotoxicity compared with the drug alone [20]. We have also demonstrated that the gold nanoparticles can be reproducibly made and are relatively stable in solution; important features for their pharmaceutical approval as drug delivery vehicles [21]. Other platinum drugs have also been successfully attached to other gold-based nanoparticles, where cellular uptake and cytotoxicity was increased compared with the free drug [22, 23].

By using both iron oxide and gold within the one drug delivery vehicle, a multifaceted system can be developed which exploits the surface chemistry of the gold whilst retaining the magnetic character of the iron oxide, allowing for biologically sound drug delivery and imaging. Lin *et al*. has demonstrated that a gold shell did not degrade the magnetic properties of their iron oxide nanoparticles [24]. A study whereby doxorubicin was successfully loaded onto gold-coated iron nanoparticles (Au@FeNPs) saw the

same retention of magnetism and a sustained release of the drug [25]. Additionally, iron oxide and gold have been used in drug delivery and imaging to form dumbbell-like particles; these studies demonstrated attachment of a range of molecules to the nanoparticles and steady drug release profiles [26, 27].

Taking the theme of this special issue (Metals in Medicine) to its limits, in this paper we give the first example of platinum anticancer drug delivery using gold-coated iron oxide nanoparticles (Figure 1). The nanoparticles have been fully characterised using dynamic light scattering (DLS), scanning transmission electron microscopy (STEM), UV visible spectrophotometry, inductively coupled plasma mass spectrometry (ICP-MS), and electron probe microanalysis (EPMA). Their cytotoxicity was evaluated using in vitro growth inhibition assays with the human ovarian cancer cell lines A2780 and A2780/cp70 and the localisation of the nanoparticles to effect site specific growth inhibition has been demonstrated using an external bar magnet.

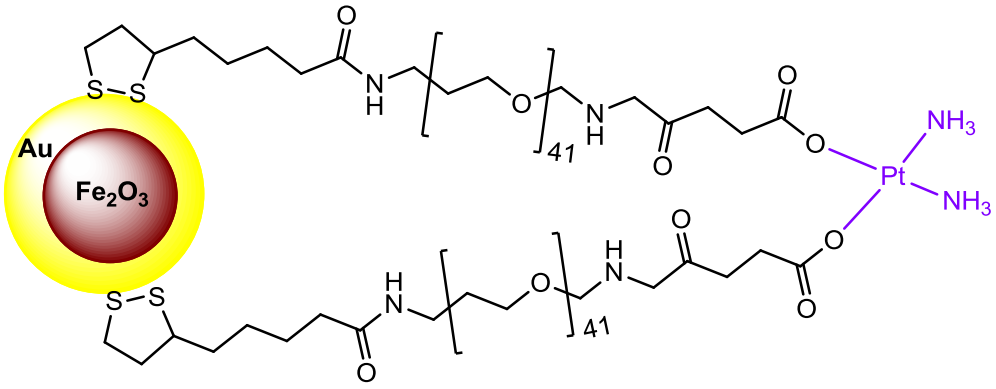

Figure 1. The nanoparticle-based drug delivery system of gold-coated iron oxide nanoparticles functionalised with a thiolated polyethylene glycol (PEG) linkers to which the active component of the anticancer drug cisplatin, $\{Pt(NH_3)_2\}^{2+}$, is attached via the terminal carboxylate groups.

2.0 Results and discussion

2.1 Nanoparticle synthesis

The synthesis of magnetite-based (Fe_3O_4) iron oxide nanoparticles is well established in the literature [13, 28]. The two most common methods for production are non-aqueous thermal decomposition and aqueous co-precipitation [29, 30]. In synthesising our nanoparticles, we first made Fe_3O_4 cores by adding NaOH to a solution of iron(II) and iron(III) chloride salts, hence utilising the co-precipitation method. The concentration and type of salts, the solution's pH and ionic strength, all contribute to the size and character of the nanoparticles created [31]. Recent literature has shown the oxidised maghemite form (γ-Fe_2O_3) preferentially binds gold compared with the magnetite form [11], and is a more stable and biocompatible form of iron oxide [31, 32]. Subsequently we used nitric acid as an oxidising agent to convert the Fe_3O_4 nanoparticles to the γ-Fe_2O_3 form (from here onwards referred to as FeNPs) [33]. Iron oxide nanoparticles are known to be unstable in solution as their agglomeration and aggregation promote particle growth, inhibiting the formation of the gold shells on their surface. Addition of tetramethylammonium hydroxide (TMAOH) facilitated dispersion of the our FeNPs, thus inhibiting aggregation and enforcing solution stabilisation through interaction between the $N(CH_3)^{4+}$ cations and the hydroxide anions that are absorbed onto the FeNP's surface [11, 34].

Initial attempts to produce a gold coating onto the FeNPs with glucose as the reducing agent, which has been used by others, saw no development of the purple/pink colour associated with metallic gold and no change in the UV spectrum, indicating that this method was unsuccessful. Instead, mixing the FeNPs with citrate anions allowed for an exchange of the adsorbed hydroxide ions [35]. Drop wise addition of $HAuCl_4$ with strong heating was then used to ensure the gold coated the iron, rather than expand its own seeds and create pure gold nanoparticles. At the end of the reaction, the presence of a purple/pink solution was indicative of a gold coating on the nanoparticles [11, 36, 37]. Pure gold nanoparticles, which may form during the coating of the FeNPs, were separated from the Au@FeNPs by use of an external magnet (Figure 2).

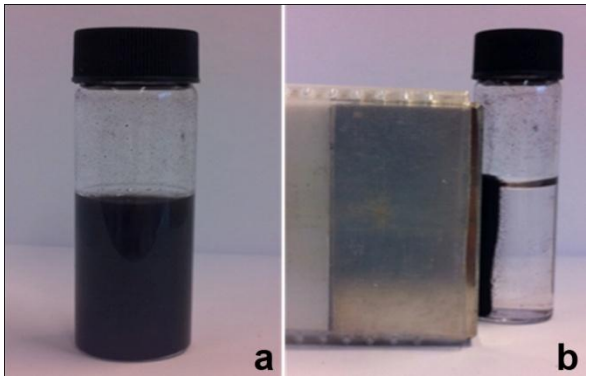

Figure 2. Photographic images of (a) gold-coated iron nanoparticles (Au@FeNP) demonstrating the purple colour associated with the presence of metallic gold and (b) the magnetic separation of the Au@FeNPs which leaves in solution any pure gold nanoparticles which form during the coating of the FeNPs.

Next, a polyethylene glycol (PEG) linker was tethered to the Au@FeNPs. Polyethylene glycol is a highly flexible and hydrophilic molecule, and has widespread pharmaceutical use due to its stability and lack of toxicity [38, 39]. Coatings of PEG on nanoparticles, polymers and liposomes can increase circulation time, improve particle stability, and when thiolated, has strong surface interactions with metallic gold creating a robust monolayer on the nanoparticles. The particular PEG linker and tethering method used here was developed and used by us previously [20, 21]. The PEG possesses a strong stabilising linkage that is hydrophobic on the inner core which then converts to hydrophilic on the outer part of the sphere, making it compatible with an aqueous environment. PEGylation of the Au@FeNPs was achieved via gentle shaking of the nanoparticles and the linker overnight, before unbound PEG linker was removed by use of an external magnet.

The final step in the synthesis of the nanoparticle system was the attachment of the platinum drug. The active component of cisplatin, $\{Pt(NH_3)_2\}^{2+}$, was coupled to the surface of the PEGylated nanoparticles

using aquated cisplatin, $[Pt(H_2O)_2(NH_3)_2]^{2+}$ and gentle shaking overnight. *N*,*N*-diisopropylethylamine (DIPEA) was used to deprotonate the carboxylic acid groups on the PEG, allowing the platinum drug to attach through strong coordination bonds, rather than weaker ionic interactions or host-guest chemistry, which alternatively has been used for platinum drugs in other systems [40-42]. Washing and magnetic separation produced the desired platinum drug tethered gold-coated iron oxide nanoparticles (Pt@Au@FeNP).

2.2. Nanoparticle Characterisation

Qualitative characterisation of the nanoparticles was accomplished by UV-visible spectrophotometry and electron probe microanalysis (EPMA) to assess the elemental presence of iron, gold and platinum. Inductively coupled plasma mass spectrometry (ICP-MS) was used to determine quantitatively the gold and platinum content. Scanning transmission electron microscopy (STEM) was used to determine nanoparticle size, morphology and dispersity.

The UV spectra of the four stages of nanoparticle synthesis: FeNPs, Au@FeNPs, PEGylated Au@FeNPs and Pt@Au@FeNPs are shown in Figure 3. The FeNPs absorb strongly up to approximately 500 nm. Upon addition of the gold coating, the strong absorption is still seen with the addition of a slight peak at ~560 nm, which is consistent with the presence of metallic gold [43]. Small diameter gold nanoparticles (i.e. ~ 15 nm) are usually observed by a peak at approximately 520 nm [43]; the observed peak at 560 nm is broad and shifted away from this wavelength due to the dielectric effect of the iron oxide. As the depth of gold coating increases in size, the iron interrupts the signal less and the peak shifts closer to 520 nm [11]. Finally, the presence of platinum is indicated by the sharp peak at approximately 220 nm [21].

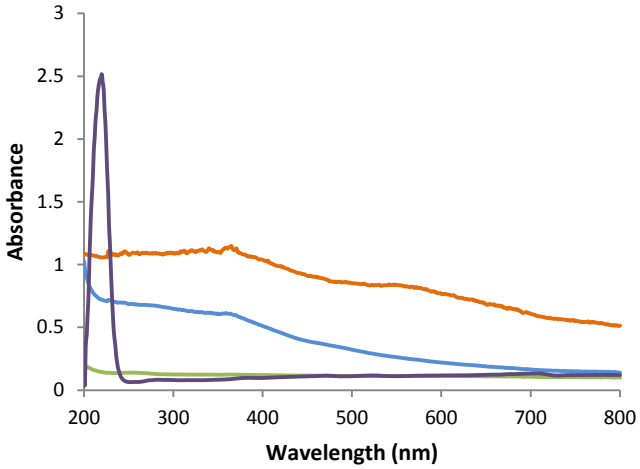

Figure 3. UV-visible spectra of the four nanoparticles: FeNP (blue), showing its strong absorption below 500 nm; Au@FeNP (orange) showing a small peak around 560 nm consistent with metallic gold; PEGylated Au@FeNP (green); and Pt@Au@FeNP (purple) showing the very strong absorption by platinum around 220 nm which swamps the absorption peaks of the iron oxide core and the gold coating. Note: different concentrations of each nanoparticle type have been used to show all peaks on scale.

Confirmation of the presence of each element in Pt@Au@FeNPs was achieved by EPMA (Figure 4). The elements iron (6.4 and 7.09 keV), gold (2.12 and 2.21 keV) and platinum (2.05 and 2.13 keV) were detected at each respective position. The relative intensities of the peaks indicate a descending concentration of iron, gold and platinum; as the iron oxide core constitutes the bulk of the nanoparticle system, accordingly it possesses the maximum elemental counts. The gold coating is thinner than the iron oxide core but considerably more abundant than the drug molecules attached and thus the platinum is consequently of significantly lower intensity. Accurate concentrations could not be determined using this technique due to the scattering effects of the round surfaces of the nanoparticles.

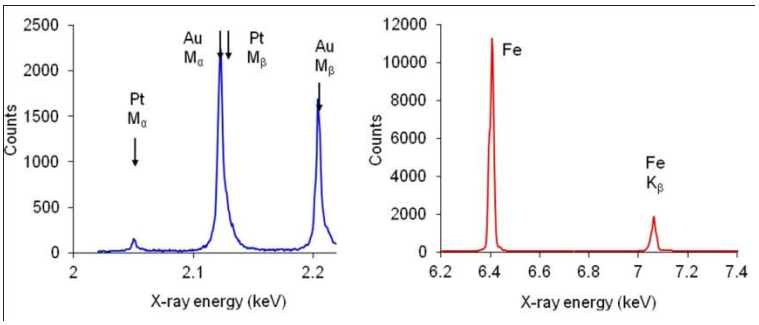

Figure 4. The electron probe microanalysis spectrum of Pt@Au@FeNPs, showing the presence of iron, gold and platinum. Scattering effects from the nanoparticles means accurate concentrations of each respective element cannot be determined.

Determination of the particle's sizes was initially attempted using dynamic light scattering although this did not prove successful due to sedimentation and/or aggregation of the particles, particularly the FeNPs; as the gold and PEG layers were attached the particles become easier to suspend in solution. In many samples a non-reproducible, bimodal distribution (not shown) was seen and it is known that DLS determined particle sizes can be affected by even the smallest amounts of aggregation in a sample [44]. Instead, scanning transmission electron microscopy (STEM) was used to determine particle sizes.

Table 1. The approximate sizes as each type of nanoparticle as determined by STEM.

Nanoparticle	**Diameter Range (nm)**
FeNP	5-50
Au@FeNP	20-80
Pt@Au@FeNP	60-120

From the STEM images, particle size distributions can be determined (Table 1). A size range of 5-50 nm was observed for the FeNPs. Whilst most of the particles had sphere-like shapes, some samples also contained rod-like structures, a phenomenon also observed by Kang *et al.* [45]. Reduction of the gold

coating onto the FeNPs results in an increase in the size of the nanoparticles to 20-80 nm. The gold coating of the Au@FeNPs is observed in the STEM images as a lightened area around the much darker iron oxide core (Figure 5). Attachment of the PEG linker and platinum drug increases the nanoparticle's size to 60-120 nm (Table 1).

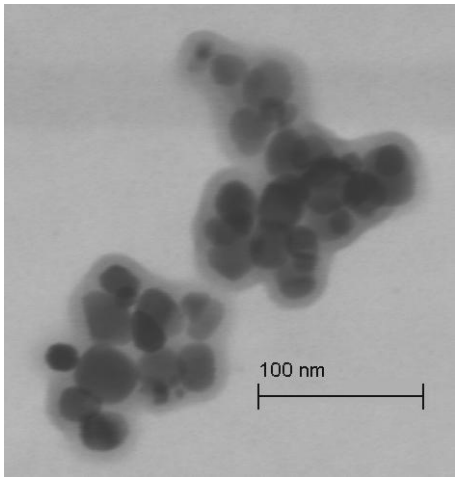

Figure 5. A scanning transmission electron microscope image of Au@FeNPs, showing the dark iron oxide core surrounded by the more transparent gold-coating.

The concentration of gold and platinum in the Pt@Au@FeNPs was quantified by ICP-MS. Each individual sample of nanoparticles contains a slightly different amount of gold and platinum, although from multiple batches there appears to be an 85% correlation between the two; increasing gold coating increases the platinum loading of the nanoparticles. The variations in concentration can arise due to slight changes in the method used to produce the gold-coating and the incubation time used to react the aquated cisplatin with the PEGylated Au@FeNPs. The concentrations obtained by ICP-MS correlate to the counts produced by EPMA (see Figure 4). Overall the loading of platinum in Pt@Au@FeNPs is 7.9 $\times 10^{-4}$ moles of platinum per gram of gold. The highest concentration of platinum obtained for the nanoparticles solutions was 8.372 μM, which is more than 50-fold higher than what we could achieve previously for pure gold-only nanoparticles: 0.135 μM platinum [21].

2.3 In vitro cytotoxicity

The cytotoxicity of the three different nanoparticles was examined using in vitro growth inhibition assays with the human ovarian carcinoma cell line A2780 and its cisplatin resistant cell line A2780/cp70. Cisplatin displays micromolar levels of cytotoxicity in the sensitive cell line and is approximately 10-fold less active in the resistant cell line. Iron oxide nanoparticles are not known to be inherently cytotoxic and in our studies no cytotoxicity was observed at concentrations up to 2 μM (note: this concentration is approximate as no reliable way of determining FeNP concentration could be found in the literature nor developed by us). The Au@FeNPs display good inherent cytotoxicity with a similar IC_{50} as cisplatin in the sensitive cancer cell line, but is 4.3-fold more active than cisplatin in the resistant line. Most importantly, the cisplatin tethered nanoparticles demonstrate activity at nanomolar concentrations and are 110-fold more active than cisplatin in A2780. This is consistent with our earlier work where oxaliplatin-based drug molecules tethered to pure gold nanoparticles were highly cytotoxic [20]. Unfortunately the cisplatin Pt@Au@FeNPs, despite having activity at nanomolar concentrations, are cross-resistant with cisplatin in A2780/cp70.

Table 2. The in vitro cytotoxicity of the nanoparticles in the human ovarian carcinoma cell line A2780 and its cisplatin resistant sub-line A2780/cp70. Resistance factor (Rf) is defined as the IC_{50} of the complex in the resistant line divided by the IC_{50} of the complex in the sensitive line; any complex with an Rf less than 1 is considered able to overcome cisplatin resistance.

Compound	**IC_{50} (μM)**		**Rf**
	A2780	**A2780/cp70**	
Cisplatin	0.527 ± 0.099	5.06 ± 0.53	9.6
FeNP	>2	>2	N/A
Au@FeNP	0.742 ± 0.148	1.62 ± 0.16	2.2
Pt@Au@FeNP	0.00467 ± 0.0008	0.0293 ± 0.041	6.3

One of the key goals of developing the iron oxide-based nanoparticles was the development of a drug delivery system that could be used to direct treatment more accurately to the sites of solid tumours by use of an external magnetic field. It was therefore important to determine whether the Pt@Au@FeNPs could be magnetically controlled in a biological environment and if localisation of the nanoparticles could induce site specific cell growth inhibition.

Cisplatin sensitive A2780 cells were grown as a monolayer in culture and treated with Pt@Au@FeNPs. The cells were then incubated in the presence of bar magnets placed under the dishes. At the conclusion of the experiment the cells were washed and stained for direct visualisation. As can be seen in figure 6, the nanoparticles were attracted to the poles of the bar magnet and the localisation that this produced resulted in growth inhibition of the cancers cells in these specific regions.

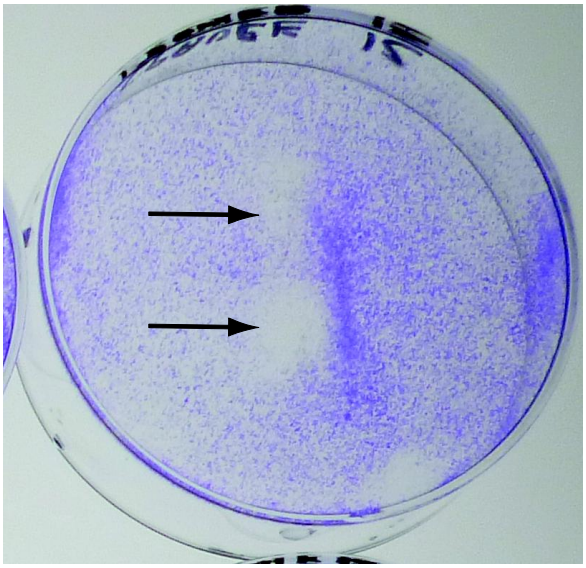

Figure 6. A representative photograph of a plate of monolayer cultured A2780 cancer cells after treatment with Pt@Au@FeNPs (12 nM) showing the growth inhibition zones from a bar magnet placed underneath the dish. The inhibition zones represent the north and south poles of the magnet to which the nanoparticles are most highly attracted.

3.0 Conclusions

Here we have successfully designed, synthesised and characterised a novel nanoparticle drug delivery system for platinum-based anticancer drugs. The nanoparticles were characterised by a number of techniques, which demonstrated a system containing a gold-coating over an iron oxide core to which the active component of cisplatin was attached using a thiolated PEG linker. These nanoparticles could be controlled and moved with an external magnetic field, allowing drug release to be localised to a specific area. Potentially, this technology could be used in patients to ensure drugs are targeted only to solid tumours, thereby leaving healthy tissue/organs intact and greatly reducing the side-effects associated with chemotherapy. The technology developed here can now be used to design further nanoparticle systems, which can examine the application of different platinum drugs, different tethering linkers and different shaped/size nanoparticles.

4.0 Methods

4.1 Materials. All chemicals and solvents were purchased from Sigma-Aldrich, except iron(III) hexahydrate and $HAuCl_4$, which were purchased from Fisher Scientific. All aqueous solutions were prepared using water filtered by a Millipore purification unit. Aquated cisplatin was made by reacting the drug with two mole equivalents of $AgNO_3$ in the dark for 48 h, before the resultant AgCl was removed using a 0.2 μm nylon filter. The PEG linker was made as previously described [20].

4.2 Inductively coupled plasma – mass spectrometry. All samples were digested in aqua regia (3:1 HCl:HNO_3) and diluted in water to a final acid content of 2%. An Agilent 7700X instrument, with a micromist nebuliser and an octapole collision cell, was calibrated using solutions prepared from a Spex CertPrep platinum standard at concentrations ranging from 0 – 1000 ppb, containing 2% nitric acid. Platinum concentration was determined using the ^{195}Pt isotope. Instrument operating conditions used were: 1,550W RF forward power, 0.85 L min^{-1} plasma carrier gas flow, 0.2 L min^{-1} makeup gas

flow, 4.6 mL min^{-1} helium gas flow in the collision cell and 0.1 rps for the nebulizer pump. Sample depth was 8 mm, sample period was 0.31 s and integration time was 0.1 s.

4.3 Dynamic light scattering. Dynamic light scattering and zeta potential experiments were conducted on a Malvern Zetasizer Nano ZS. The machine was calibrated using a 60 nm polystyrene standard. Each 1 mL sample was loaded into a cell and particle size and zeta potential were measured simultaneously 3 times with triplicate samples.

4.4 Scanning transmission electron microscopy. Samples of FeNP, Au@FeNP, PEGylated Au@FeNP, and Pt@Au@FeNP (1 μL) were dried on a silicon substrate and placed under vacuum. TEM images were collected using a Zeiss ULTRA plus, high resolution Schottky field-emission scanning electron microscope. An accelerating voltage of 30 kV was applied to each sample. A STEM detector was used for both brightfield and darkfield images.

4.5 Ultraviolet-visible spectrophotometry. UV-visible spectra were obtained using a Varian Cary 50 Bio spectrophotometer running CaryWin UV scan software. Each sample (2 mL) was prepared at appropriate dilutions to achieve absorption values between 0 – 1. Samples were measured in a silica cuvette (1 cm) and an average of three measurements were used.

4.6 Electron probe microanalyser. A sample of Pt@Au@FeNPs (1 μL) was dried on a silicon substrate and placed under vacuum. The wavelength-dispersive X-ray spectrum was acquired in a Cameca SX100 electron probe microanalyser using a pentaerythritol crystal with a lattice spacing of 2d, 8.75 Å at 20 keV, and a 40 nA electron beam.

4.7 Synthesis of iron nanoparticles (FeNP). All glassware used in the preparation of nanoparticles was soaked in aqua regia for at least 4 h and rinsed with distilled water until the water pH was neutral. $FeCl_2$ (5.4 g, 0.042 mol) and $FeCl_3$ (2.0 g, 0.013 mol) were dissolved in a three neck round bottom flask in 20 mL distilled water and HCl (100 µL, 2 M). This was stirred by a double-linked glass stirrer, using a mechanical stirrer (Janke & Kunkel, Type RW20, speed setting "2") until the salts dissolved. The entire pre-synthesised stock solution was added drop wise to NaOH (250 mL, 1.5 M), whilst being continuously stirred (speed setting "4.5"). The solution turned dark black as the nanoparticles formed. The FeNPs were collected using a permanent magnet and the supernatant discarded. They were then washed gradually with HNO_3 (400 mL, 0.1 M) and HNO_3 (200 mL, 0.01 M) before being suspended in HNO_3 (100 mL, 0.01 M). This solution was heated to 90 ^oC and stirred constantly (speed setting "2") for 30 min until the solution turned a brown-red colour. After cooling the particles were washed 3 times with distilled water and separated from the solution using a permanent magnet, and then resuspended in 0.1 M TMAOH.

4.8 Gold coating of iron oxide nanoparticles (Au@FeNP). Iron oxide nanoparticles (10 mL, unknown concentration) were added to sodium citrate (100 mL, 0.1 M) in a three neck round bottom flask and stirred for 30 min (speed setting "5"). The solution was sonicated for 15 min before being heated to boiling point with a bunsen burner, with continuous heating, 100 µL aliquots of $HAuCl_4$ (15 mL, 1% w/v) was added every minute. The Au@FeNPs were then separated from any pure gold nanoparticles using a permanent magnet and washed with distilled water three times before being redispersed in water.

4.9 Assembly of cisplatin-tethered gold-coated iron oxide nanoparticles (Pt@Au@FeNP). Gold-coated iron oxide nanoparticles (200 µL, unknown concentration), were diluted to 1 mL in a glass vial by the addition of distilled water (700 µL) and PEG linker (100 µL, 10 mM). This was then placed in round bottom flask and spun on rotary evaporator for 12 h to form a PEG monolayer on the surface of

the nanoparticles. Unbound PEG linker was removed using a permanent magnet to separate the PEGylated Au@FeNPs from the supernatant. The PEGylated nanoparticles were then redispersed in 1 mL distilled water and the purification completed once more. A 0.1 M stock solution of *N*,*N*-diisopropylethylamine (DIPEA) was prepared by dissolving 17 µL of the base 1,3-dimethyl-3,4,5-tetrahydro-2(1H)-pyrimidone in 1 mL DIPEA. Of this, 100 µL was added to a glass vial containing PEG bound gold-coated iron nanoparticles. Aquated cisplatin (2.5 mg) was dissolved in 1 mL 1,3-dimethyl-3,4,5-tetrahydro-2(1H)-pyrimidone and an aliquot (100 µL) of this added to the nanoparticles, before being gently shaken overnight. Finally, the Pt@Au@FeNPs were separated from the supernatant using a permanent magnet and washed twice with distilled water before being redispersed in the same medium.

4.10 Cytotoxicity and drug localisation experiments. In vitro growth inhibition assays were conducted as previously described [46], with the platinum and gold concentrations of the nanoparticles determined using ICP-MS for each individual batch used in the cytotoxicity assays. For the magnetic susceptibility and localisation experiments A2780 cells were plated at a density of 50,000 cells per 6 cm petri nunc tissue culture dish and grown for 24 h before the cells were then incubated with Pt@Au@FeNPs at a concentration of either 6 or 12 nM and in the presence or absence of a bar magnet (18 × 4 mm). To ensure the magnets did not move and the dishes remained flat during incubation, they were covered in bubble wrap with the magnets nestled between the bubbles. After 24 h the drug media was removed and fresh medium added for a further 48 h of incubation. Finally, the dishes were washed with phosphate buffered saline, fixed twice for 5 min in methanol, dried in air, then stained with crystal violet for 5 min. Unbound stain was washed off with water before photographic images were obtained.

Acknowledgements

We acknowledge the facilities, and the scientific and technical assistance, of the Australian Microscopy & Microanalysis Research Facility at the Australian Key Centre for Microscopy and Microanalysis, The

University of Sydney. This work was supported by a Scottish Crucible grant; the funding source had no involvement in: the collection, analysis and interpretation of the data; writing the article, nor any decision to submit the article for publication.

References

[1] N. J. Wheate, S. Walker, G. E. Craig and R. Oun, Dalton Trans., 39 (2010) 8113-8127.

[2] L. Kelland, Nat. Rev. Cancer, 7 (2007) 573-584.

[3] T. W. Hambley, Science, 318 (2007) 1392-1393.

[4] J. Reedijk, Chem. Rev., 99 (1999) 2499-2510.

[5] A. V. Klein and T. W. Hambley, Chem. Rev., 109 (2009) 4911-4920.

[6] A.-M. Florea and D. Büsselberg, Cancers, 3 (2011) 1351-1371.

[7] V. Torchilin, Adv. Drug Del. Rev., 63 (2011) 131-135.

[8] C. C. Berry, J. Mater. Chem., 15 (2005) 543-547.

[9] G. F. Goya, T. S. Berquo, F. C. Fonseca and M. P. Morales, J. Appl. Phys., 94 (2003) 3520-3528.

[10] M. K. Yu, Y. Y. Jeong, J. Park, S. Park, J. W. Kim, J. J. Min, K. Kim and S. Jon, Angew. Chem. Int. Ed., 47 (2008) 5362-5365.

[11] J. L. Lyon, D. A. Fleming, M. B. Stone, P. Schiffer and M. E. Williams, Nano Lett., 4 (2004) 719-723.

[12] E. E. Carpenter, S. Calvin, R. M. Stroud and V. G. Harris, Chem. Mater., 15 (2003) 3245-3246.

[13] U. Jeong, X. Teng, Y. Wang, H. Yang and Y. Xia, Adv. Mater., 19 (2007) 33-60.

[14] M. Babincová, V. Altanerová, C. Altaner, C. Bergemann and P. Babinec, IEEE Trans. Nanobiosci., 7 (2008) 15-19.

[15] M. Kettering, H. Zorn, S. Bremer-Streck, H. Oehring, M. Zeisberger, C. Bergemann, R. Hergt, K.-J. Halbhuber, W. A. Kaiser and I. Hilger, Phys. Med. Biol., 54 (2009) 5109-5121.

[16] S. Likhitkar and A. K. Bajpai, Carbohydr. Polym., 87 (2012) 300-308.

[17] E. E. Connor, J. Mwamuka, A. Gole, C. J. Murphy and M. D. Wyatt, Small, 1 (2005) 325-327.

[18] K. B. Male, B. Lachance, S. Hrapovic, G. Sunahara and J. H. T. Luong, Anal. Chem., 80 (2008) 5487-5493.

[19] P. S. Ghosh, C.-K. Kim, G. Han, N. S. Forbes and V. M. Rotello, ACS Nano, 2 (2008) 2213-2218.

[20] S. D. Brown, P. Nativo, J.-A. Smith, D. Stirling, P. R. Edwards, B. Venugopal, D. J. Flint, J. A. Plumb, D. Graham and N. J. Wheate, J. Am. Chem. Soc., 132 (2010) 4678-4684.

[21] G. E. Craig, S. D. Brown, D. Lamprou, D. Graham and N. J. Wheate, Inorg. Chem., 51 (2012) 3490-3497.

[22] T. S. Hauck, T. L. Jennings, T. Yatsenko, J. C. Kumaradas and W. C. W. Chan, Adv. Mater., 20 (2008) 3832-3838.

[23] S. Dhar, W. L. Daniel, D. A. Giljohann, C. A. Mirkin and S. J. Lippard, J. Am. Chem. Soc, 131 (2009) 14652-14653.

[24] J. Lin, W. Zhou, A. Kumbhar, J. Wiemann, J. Fang, E. E. Carpenter and C. J. O'Connor, J. Solid State Chem., 159 (2001) 26-31.

[25] S. Kayal and R. V. Ramanujan, J. Nanosci. Nanotechnol., 10 (2010) 5527-5539.

[26] C. Xu, B. Wang and S. Sun, J. Am. Chem. Soc, 131 (2009) 4216-4217.

[27] J.-S. Choi, Y.-w. Jun, S.-l. Yeon, H. C. Kim, J.-S. Shin and J. Cheon, J. Am. Chem. Soc., 128 (2006) 15982-15983.

[28] D. L. Huber, Small, 1 (2005) 482-501.

[29] S.-J. Cho, J.-C. Idrobo, J. Olamit, K. Liu, N. D. Browning and S. M. Kauzlarich, Chem. Mater., 17 (2005) 3181-3186.

[30] O. A. Loaiza, E. Jubete, E. Ochoteco, G. Cabanero, H. Grande and J. Rodriguez, Biosens. Bioelectron., 26 (2011) 2194-2200.

[31] V. I. Shubayev, T. R. Pisanic and S. Jin, Adv. Drug Del. Rev., 61 (2009) 467-477.

[32] A. K. Gupta and M. Gupta, Biomaterials, 26 (2005) 3995-4021.

[33] S. Lefebure, E. Dubois, S. Neveu and R. Massart, J. Mater. Res., 13 (1998) 2975-2981.

[34] R. Massart, IEEE Trans. Magn., 17 (1981) 1247-1248.

[35] J. L. Lyon, D. A. Fleming, M. B. Stone, P. Schiffer and M. E. Williams, Nano Letters, 4 (2004) 719-723.

[36] P. G. Rudakovskaya, E. K. Beloglazkina, A. G. Majouga and N. V. Zyk, Mendeleev Commun., 20 (2010) 158-160.

[37] J. Jeong, T. H. Ha and B. H. Chung, Anal. Chim. Acta, 569 (2006) 203-209.

[38] D. E. Owens and N. A. Peppas, Int. J. Pharm., 307 (2006) 93-102.

[39] S. E. Barry, Int. J. Hyperthermia, 24 (2008) 451-466.

[40] M. J. Pisani, N. J. Wheate, F. R. Keene, J. R. Aldrich-Wright and J. G. Collins, J. Inorg. Biochem., 103 (2009) 373-380.

[41] A. M. Krause-Heuer, N. J. Wheate, M. J. Tilby, D. Pearson, C. J. Ottley and J. R. Aldrich-Wright, Inorg. Chem., 47 (2008) 6880-6888.

[42] S. Walker, R. Oun, F. J. McInnes and N. J. Wheate, Isr. J. Chem., 51 (2011) 616-624.

[43] S. Link and M. A. El-Sayed, J. Phys. Chem. B, 103 (1999) 4212-4217.

[44] B. J. Frisken, Appl. Opt., 40 (2001) 4087-4091.

[45] Y. S. Kang, S. Risbud, J. F. Rabolt and P. Stroeve, Chemistry of Materials, 10 (1998) 1733-1733.

[46] G. J. Kirkpatrick, J. A. Plumb, O. B. Sutcliffe, D. J. Flint and N. J. Wheate, J. Inorg. Biochem., 105 (2011) 1115-1122.